Nuclear Instruments and Methods in Physics Research B 267 (2009) 1623–1625

Contents lists available at ScienceDirect

Nuclear Instruments and Methods in Physics Research B

journal homepage: www.elsevier.com/locate/nimb

High concentration Mn ion implantation in Si

Nianhua Peng [a,*], Christopher Jeynes [a], Melanie J. Bailey [a], Damitha Adikaari [b], Vlad Stolojan [b], Roger P. Webb [a,b]

[a] Surrey Ion Beam Centre, Surrey University, Guildford GU2 7XH, UK
[b] Advanced Technology Institute, Surrey University, Guildford GU2 7XH, UK

ARTICLE INFO

Article history:
Available online 30 January 2009

PACS:
61.72.uf
75.50.Pp

Keywords:
Dilute magnetic semiconductor
Ion implantation
Si
Mn doping

ABSTRACT

Recent controversial reports of possible above room temperature ferromagnetism in high dose Mn implanted Si samples was the motivation for examining this interesting Mn–Si binary system. 50 keV Mn^+ ions were implanted into n-type CZ (001) Si wafers up to 5×10^{16} ions/cm^2 at room temperature, leading to the formation of disordered surface Mn/Si layers. The Mn implanted samples were subjected to further treatments by pulsed laser annealing in air. The distribution and evolution of the Mn dopant in the Si host upon thermal treatments is characterized by Rutherford backscattering, cross-sectional transmission electron microscopy and Raman scattering measurements.

1. Introduction

Ferromagnetic semiconductors, in particular those based on Si and GaAs with high Curie temperatures, are needed for novel device fabrication with high operating speed and new functionality. In 2000, a theoretical calculation by Dietl et al. [1] showed that the Curie temperature above 300 K could be achieved in some conventional p-type doped compound semiconductors through doping of Mn of up to a few percent in atomic concentration, while a much lower Curie temperature was predicted for high dose Mn doping in p-type Si. Ferromagnetism has also been predicted from density functional theory calculations for Mn substitutional doping in Si [2]. A recent theoretical study based on first principle total energy calculations suggested that high level Mn doping in Si could be achieved under non-equilibrium growth conditions [3].

In fact, under thermal equilibrium conditions, the solubility of Mn in Si is far too low for a macroscopic ferromagnetic ordering, and Mn silicides can easily be formed at high Mn doping levels. Among all non-equilibrium Mn doping methods, ion implantation is unique due to its compatibility with current microelectronics fabrication technology. Until now, experimental reports on Mn doped ferromagnetic Si through ion implantation are limited and somewhat controversial. For example, claims of above room temperature ferromagnetism have been made in a few studies of both n-type and p-type Si samples implanted with Mn ions, followed by rapid thermal annealing in the forming gas atmosphere [4,5]. However, a more recent study failed to confirm the above room temperature ferromagnetism introduced by Mn doping in p-type Si samples prepared under identical experimental conditions, where the formation of Mn silicide segregation is evident [6]. Compared to rapid thermal annealing of ion implanted samples, pulsed laser annealing seems to be a more suitable method in avoiding the formation of unwanted Mn silicides, as revealed by a recent report on high Mn doping in GaAs [7]. This motivates us to examine the effect of pulsed laser annealing on the possible growth of Mn silicides in high dose Mn implanted Si.

2. Experiment

2.1. Sample preparation

A commercial n-type Czochralski (CZ) (001) Si wafer was implanted at room temperature with a single energy of 50 keV Mn^+ ions to a dose of 5×10^{16} ions/cm^2, using the Danfysik implanter at the Surrey Ion Beam Centre. This implant gives a very high peak volume Mn concentration in Si host lattice, but also a range of low Mn dopant concentrations over all the implanted depth. The Si samples were titled by 7° in order to reduce lattice channeling effects. The implantation area was defined by a Si aperture, and the Mn^+ ion beam current on the sample plate was 50 μA.

Mn ion implanted samples were irradiated in air with a single 340 mJ/cm^2 pulse from a Lambda Physik LPX 200 KrF excimer laser with $\lambda = 248$ nm and a full width at half maximum (FWHM) = 25 ns. The laser beam had been homogenized to a beam

* Corresponding author. Tel.: +44 1483 682282; fax: +44 1483 686091.
E-mail address: n.peng@surrey.ac.uk (N. Peng).

0168-583X/$ - see front matter © 2009 Elsevier B.V. All rights reserved.
doi:10.1016/j.nimb.2009.01.065

spot size of 5 mm by 5 mm with a spatial uniformity of 10%. For comparison, selected samples were also annealed by rapid thermal annealing at 800 °C for 5 min in 5% H_2/N_2 forming gas atmosphere.

The implantation dose, damage and uniformity of Mn dopant in Si was examined by Rutherford backscattering spectroscopy (RBS) and channeling (c-RBS) using 1.5 MeV He^+ ions on line 4 of the 2 MV Tandem accelerator at the Surrey Ion Beam Centre. Collected RBS data were then analyzed using the Datafurnace software code [8]. In addition to two RBS detectors arranged in IBM and Cornell geometries respectively, a Si–Li X-ray detector (50 mm^2, 150 eV resolution) was also used to collect He^+ particle induced X-ray emissions (PIXE).

Further characterization on the ion implantation damage and recrystallisation after annealing was carried out on a Systems 2000 Renishaw Raman microscope. The samples were placed underneath optical objectives with a magnification of 50× and were excited by a green 514 nm laser directed through the microscope. The 180° backscattered light was collected along the same optical path as the incoming laser and detected by charge coupled device array detectors after dispersion through a monochromator.

Cross sectional transmission electron microscope (XTEM) analysis was performed on a Hitachi HD2300A scanning transmission electron microscopy (STEM) with a Schottky field emitter operating at 200 kV. A Gatan Enfina electron energy loss spectrometer (EELS) and an EDAX energy dispersive X-ray spectrometer (EDX) fitted with this STEM were also used for chemical composition analysis at nanometer scale.

3. Results and discussion

Except for a very thin layer of surface native oxide, the virgin Si wafers were shown to be free from any metal impurities as revealed by both RBS and particle induced X-ray emission (PIXE) spectra. Mn ion implantation and post implant annealing processes did not introduce any extra metal impurities.

Mn ion implantation produced significant lattice damage in Si, leading to the formation of a completely disordered surface Si/Mn layer. Raman spectra of as implanted (data series 1) and pulsed laser annealed (data series 2) samples are presented in Fig. 1, together with the Raman spectrum from a pure Si (data series 3) sample. The spectrum of the as implanted sample is very similar to that reported previously for an amorphous Si sample [9]. The spectrum from the pulsed laser annealed sample is clearly a mixture of spectra from completely disordered and perfect crystal samples, except the small shift in peak position at a wave number of around 521 cm^{-1}. In contrast to pulsed laser annealing, the rapid thermally annealed samples show better overall recrystallisation, as revealed by the well defined crystal-like Raman spectra (not shown).

These observations of ion implantation introduced amorphisation and regrowth after annealing by Raman spectroscopy are confirmed by the RBS and c-RBS data (not shown here). In Fig. 2, we show the RBS spectra due to Mn dopant in as implanted (data series B27s) and pulsed laser annealed (data series B27r) samples. The distribution of the Mn dopant is approximately Gaussian for the as implanted sample, while a broadening of Mn distribution and a reduction in peak Mn concentration upon pulsed laser annealing are clearly presented in data series B27r, indicating the diffusion of Mn dopant upon the laser annealing process.

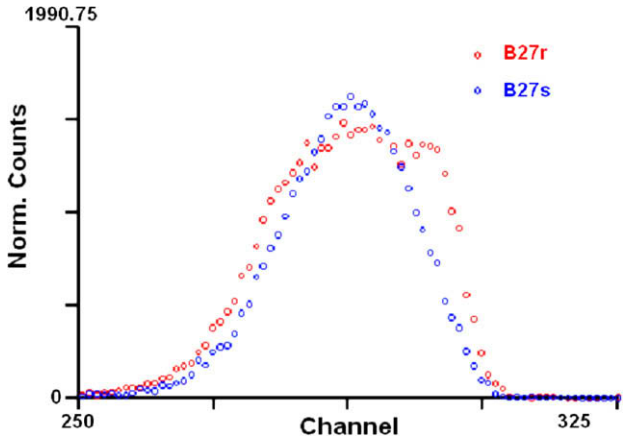

Fig. 2. RBS data from Mn dopants for as implanted (data series B27s) and pulse laser annealed (data series B27r) samples, with Mn implantation dose of 5×10^{16} ions/cm^2.

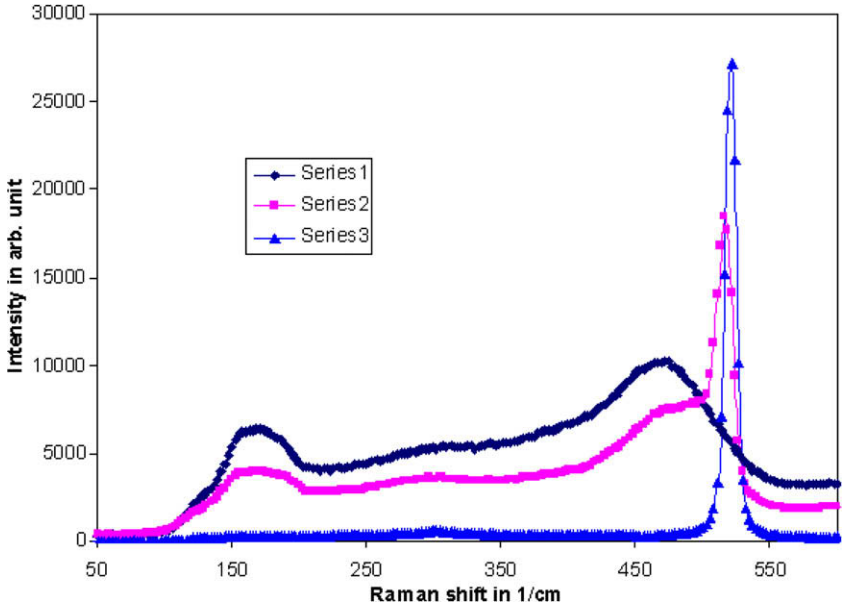

Fig. 1. Raman scattering spectra for 5×10^{16} ions/cm^2 Mn implanted (series 1), pulsed laser annealed (series 2) and virgin Si (series 3) wafers.

Fig. 3. XTEM HAADF image from 5×10^{16} ions/cm^2 Mn ion implanted sample after pulsed laser annealing in air.

In Fig. 3, we show a high angle annular dark field (HAADF) image obtained from a pulse laser annealed Mn implanted sample. Interestingly, the implanted region is crystallized after a single pulse of laser annealing, and Si crystallites of about 30 nm in diameter are present. The increased intensity at the grain boundaries is very likely to be due to the accumulation of Mn at the boundaries, since Mn is heavier than Si. This accumulation of Mn near the grain boundary is also visible near the surface of the sample, where the implanted Mn dopant concentration is much lower than that in the projected peak implantation depth of about 50 nm. EDX and EELS mappings across grain boundaries give further evidence of Mn segregation. Additionally, the thickness of the Mn-rich region is estimated to be about 5 nm. The nanodiffraction pattern from a region of about 3 nm at the grain boundary can be indexed as due to Mn_5Si_3 [10]. It is of interest to note the different morphology observed here compared to those reported before [4–6], possibly due to different sample preparation conditions.

The Mn ion energy was chosen in this study so that the penetration depth of the KrF excimer laser would be able to cover the depth of damage created by the implantation process [11,12]. Surface oxide layer should also be well separated from Mn dopants. Ideally, pulsed KrF excimer laser annealing would cause the implanted surface layer to melt and recrystallize upon solidification within a very short timescale, providing an opportunity for Mn substitution for Si, but with limited thermal energy for Mn diffusion and segregation. These RBS, Raman and XTEM observations reveal that the Mn-rich silicide phase had been segregated from the Si matrix and that Mn diffusion occurs after a single pulse of laser annealing in this high dose Mn implanted samples. It is not clear whether high level substitutional Mn dopants exist in the Si matrix or not at this stage of our research, though the shift in Raman scattering peak at wave number around 521 cm^{-1} in Fig. 1 might be an indication for Mn substituting for Si.

For the proposed application of ferromagnetic semiconductors in spintronics devices, a polycrystalline Si/Mn is not as attractive as a highly crystalline Si/Mn. This implantation work, carried out at a nominal room temperature, clearly lead to the destruction of crystalline Si host and the formation of nano crystallites with dimensions down to 30 nm after pulsed laser annealing. Even with ion implantations carried at 350 °C as reported before, post implant annealing was still required for removing the lattice damage created by implantation process [4,6]. Further research on the ion implantation and annealing conditions is necessary to achieve high level Mn substitution for Si while maintaining a highly crystalline host lattice structure.

4. Conclusions

In this brief report, we have shown from our experimental observations based on RBS, Raman and XTEM, that pulsed laser annealing leads to significant Mn dopant diffusion and Mn-rich silicide phase segregation around the surface of nano Si crystallites in high dose Mn ion implanted Si samples. The difference in microstructure observed here to those reported previously is likely to be due to different sample preparation conditions. The peak position shift at wave number around 521 cm^{-1} in Raman spectra for the Mn implanted samples compared to a virgin Si sample might be an indication for Mn substitutional doping in Si, but more detailed work is necessary for a quantitative estimation.

Acknowledgements

We would like to thank EPSRC (EP/D032210) for funding the Surrey Ion Beam Centre. Nianhua Peng would like to thank Alex Royal for his help with Mn ion implantation and Dr. Simon Henley and Chris Buxey for their assistance on Raman data collection.

References

[1] T. Dietl, H. Ohno, F. Matsukura, J. Cibert, D. Ferrand, Science 287 (2000) 1019.
[2] F. Bernardini, S. Picozzi, A. Continenza, Appl. Phys. Lett. 84 (2004) 2289.
[3] X. Luo, S.B. Zhang, S.H. Wei, Phys. Rev. B 70 (2004) 033308.
[4] M. Bolduc, C. Awo-Affouda, A. Stollenwerk, M.B. Huang, F.G. Ramos, G. Agnello, V.P. LaBella, Phys. Rev. B 71 (2005) 033302.
[5] P.R. Bandaru, J. Park, J.S. Lee, Y.J. Tang, L.H. Chen, S. Jin, S.A. Song, J.R. O'Brien, Appl. Phys. Lett. 89 (2006) 112502.
[6] S. Zhou, K. Potzger, G. Zhang, A. Mucklich, F. Eichhorn, N. Schell, R. Grotzschel, B. Schmidt, W. Skorupa, M. Helm, J. Fassbender, D. Greiger, Phys. Rev. B 75 (2007) 085203.
[7] O.D. Dubon, M.A. Scarpulla, R. Farshchi, K.M. Yu, Phys. B 376–377 (2006) 630.
[8] N.P. Barradas, C. Jeynes, R.P. Webb, Appl. Phys. Lett. 71 (1997) 291.
[9] R. Alben, D. Weaire, J.E. Smith Jr., M.H. Brodsky, Phys. Rev. B 11 (1975) 2271.
[10] V. Stolojan, Microsc. Anal. 22 (2008) 15.
[11] R.P. Webb, in: D. Briggs, M.P. Seah (Eds.), Practical Surface Analysis, second ed., John Wiley & Sons, Ltd., 1983, p. 604.
[12] H.R. Philipp, E.A. Taft, Phys. Rev. 120 (1960) 37.